Biointerface Research in Applied Chemistry
Open-Access Journal (ISSN: 2069-5837)

*Article*
**Volume 13, Issue 5, 2023, 490**
https://doi.org/10.33263/BRIAC135.490

# Modeling of Adsorption of Copper on Activated Leaf-Based Biomass using Response Surface Methodology (RSM)

**Yudi Sukmono [1], Wei Jie Ngu [2], Tony Hadibarata [2,*], Muhammad Syafrudin [3]**

[1] Industrial Engineering Program, Faculty of Engineering, Mulawarman University, Samarinda, Indonesia
[2] Environmental Engineering Program, Faculty of Engineering and Science, Curtin University, CDT250, Miri 98009, Malaysia
[3] Department of Artificial Intelligence, Sejong University, Seoul 05006, Korea
* Correspondence: hadibarata@curtin.edu.my (T.H.);

Scopus Author ID 16233109100
**Received: 9.08.2022; Accepted: 4.10.2022; Published: 6.01.2023**

**Abstract:** Due to rapid development, heavy metal pollution has resulted in water pollution, causing a reduction in water sources. Hence, remediation actions should be taken to remove heavy metals. Adsorption is a physical remediation that is cost-effective and efficient in heavy metal removal. Developing adsorbents from low-cost materials, including leaves, could reduce the remediation cost. In this research, four types of leaves were collected and activated chemically into the adsorbents. The adsorbent with the highest adsorption capacity was determined through adsorbent screening, and the selected adsorbent was used in the following equilibrium study, batch study, and Fourier-Transform Infrared Spectroscopy analysis. Central composite design in Design Expert was used to design the batch study. Mango leaves adsorbent was found to have the highest adsorption capacity. The equilibrium time for copper and lead adsorptions was found to be 20 minutes and 30 minutes, respectively. The functional groups on adsorbents were identified by FTIR analysis. The fittest adsorption isotherm and adsorption kinetics were found to be Langmuir isotherm and Pseudo-second-order kinetic model. The Langmuir adsorption capacity constant was found as 12.7139 mg/g for copper adsorption. This leaf powder is valuable since they are green, economical, and easy to prepare with a simple design biosorption technique.

**Keywords:** adsorption; chemical activation; heavy metal remediation; low-cost adsorbents.



## 1. Introduction

Rapid development has resulted in the pollution of precious water sources. One of the water pollutants is heavy metal, which refers to a group of metals or metalloids that are four times denser than water. Weathering of bedrock, which contains heavy metals, will indirectly release the heavy metals into the environment [1, 2]. Nevertheless, the main contributor to heavy metal pollution is anthropogenic activities. Adsorption is a cost-effective remediation method that is efficient in heavy metal removal and flexible enough to be used in different working conditions [3-5]. Therefore, this research studies the adsorption of heavy metals by using adsorbents developed from leaves. Developing adsorbents from low-cost materials, such as leaves, could help reduce the manufacturing costs of adsorbents and the remediation costs of adsorption.

Among the 28000 species on the Earth, around 33% of the species depend on freshwater for survival. Freshwater pollution has greatly reduced the species' survival chances, which may eventually lead to their extinction, causing ecosystem imbalance. Anthropogenic activities are the main cause of the increment of heavy metals in the environment. Untreated effluent discharge from industries such as tannery-related industries and municipal sewage will contribute to the increment of heavy metal ions in the environment [6, 7]. Furthermore, the mining industry's tailings, which contain high heavy metal concentrations, will cause severe heavy metal pollution to nearby land if not properly treated. When fungicides and organic or inorganic fertilizers are applied to agricultural land, the copper concentration in the soil rises, resulting in copper pollution of the farmland. Heavy metal pollution is very dangerous to humans and the environment due to its high toxicity [8-10]. Without proper remediation actions, the heavy metals in the environment will eventually affect human health through food chains in an ecosystem, apart from disturbing the natural ecosystem. Copper is one of the heavy metals found in the environment that is a micronutrient for the human body. To maintain a healthy life, 0.9 mg/L of copper is required for an adult. As a micronutrient, copper will act as a cofactor in catalyzing enzyme actions in the human body [8]. However, heavy metal pollution in the environment has increased the risk of copper over intake, causing copper accumulation in the human body. The common symptoms of copper poisoning include vomiting, diarrhea, nausea, and abdominal pain, but severe copper poisoning will cause organ damage and even organ functionality failure [10]. The presence of inorganic copper in the body of an individual who has high homocysteine levels will increase the risk of Alzheimer's disease [11]. Copper ions in the human body could cause oxidative damage to the DNA by producing reactive oxygen species that cause structural damage to the biomolecules [11-13]. Consequently, human health will be negatively affected when an individual.

Heavy metal pollution will have a negative effect on the natural ecosystem through bioaccumulation and biomagnification. Bioaccumulation allows heavy metals to be accumulated in the bodies of organisms, while biomagnification will amplify the heavy metal concentration in the bodies of organisms along the food chain [13], causing consumers at higher trophic levels to have higher heavy metal levels in their bodies. High copper concentration exposure will trigger mucus secretion for *Scutus* species to prevent the entry of heavy metals into the gills, but the mucus could cause osmoregulatory disruption [14]. When the soil copper concentration exceeds 100 mg/kg, crop yields for rice plants are found to be reduced by 10%, and further increment of the soil copper concentration has led to a further reduction of crop yields [15]. The adsorbents used in adsorption could be prepared through chemical activation, physical activation, or a combination of both. For chemical activation, dehydrating chemicals will be used to carbonize and perform pyrolysis of carbon-rich organic materials simultaneously, while physical activation requires the carbonization and thermal activation to be carried out separately at high temperatures [16-18]. The objectives of this research include determining the adsorption capacity of copper by the adsorbents, identifying the surface chemistry of adsorbents in the adsorption process, and investigating adsorption isotherms and adsorption kinetics of the adsorbents.

## 2. Materials and Methods

*2.1. Adsorbate and adsorbent preparation.*

Copper sulfate and other solvents and chemicals were purchased from Sigma Aldrich (St. Louis, USA). Stock solutions for Copper (II) sulfate were prepared from 500 mg/L of copper ions and 1.3 g of copper (II) sulfate in 1 liter of ultrapure water, respectively. Chemical activation is chosen to produce the adsorbents from the leaves collected, including decorative palm leaves, longan leaves, mango leaves, and pineapple leaves. The collected leaves are cleaned and dried separately in an oven at 105 °C until a constant mass is achieved. The dried leaves are ground into powder using a blender separately. The leaf powder will be activated chemically in a furnace using sodium hydroxide with an impregnation ratio of 1: 1 at 600°C. The adsorbents produced are washed with 1 M hydrochloric acid and then rinsed with hot ultrapure water until the pH is within 6.5–7 [19-21]. The rinsed adsorbents were dried and stored in separate zipper bags. Adsorbent screening is important to identify the adsorbents with the highest adsorption capacity among the four types of adsorbents produced. The selected adsorbents were used in the following experiments: The adsorption conditions are standardized at 0.01 g of adsorbents, 100 mL of 50 mg/L copper (II) sulfate solution, agitation speed of 150 rpm, and contact time of 15 minutes. The final copper concentration was determined using Atomic Adsorption Spectroscopy (AAS), and the adsorption capacity was calculated using Equation 1:

$$Adsorption\ capacity = \frac{C_i - C_f}{m} \times V \quad (1)$$

where adsorption capacity is in mg/g, $C_i$ is the initial heavy metal concentration in mg/L, $C_f$ is the remaining heavy metal concentration after adsorption in mg/L, m is the adsorbent dosage in g, and V is the volume of heavy metal solution in L.

*2.2. Batch study.*

An equilibrium study will be conducted to investigate both equilibrium time and equilibrium concentration. For equilibrium time determination, the heavy metal concentration, adsorbent dosage, and agitation speed will be kept constant while the contact time will be altered. In this research, 100 mL of heavy metal solution is set at 30 mg/L of concentration, the adsorbent dosage is set at 0.03 g, and the agitation speed is set at 150 rpm. After the determination of equilibrium time, the contact time will be standardized at equilibrium time, and the initial heavy metal concentration will be replaced with 10 mg/L, 20 mg/L, 40 mg/L, and 50 mg/L to find the equilibrium concentration. The batch study in this research was designed using the Central Composite Design function in Design Expert software. The maximum and minimum values of each parameter are inputted into Design Expert for experiment design, as shown in Table 1. The batch study will be carried out based on the parameters generated by the design expert.

**Table 1.** Data input for Central Composite Design in Design Expert.

| Batch | Agitation speed, rpm | | Contact time, min | | Adsorbent dosage, g | | Initial heavy metal concentration, mg/L | |
|---|---|---|---|---|---|---|---|---|
| | Low | High | Low | High | Low | High | Low | High |
| Copper | 100 | 200 | 10 | 30 | 0.01 | 0.05 | 10 | 50 |

*2.3. FTIR analysis.*

The surface functional groups of adsorbents were determined using Fourier Transform Infrared Spectroscopy (FTIR) analysis (Agilent Model: Cary 630). It was detected in the spectral range between 650 and 4000 $cm^{-1}$.

*2.4. Adsorption isotherms and adsorption kinetics.*

Adsorption isotherm was used to determine the adsorption equilibrium and the adsorption capacity of the adsorbents, whereas adsorption kinetic was used to determine the adsorption rate at the solid-liquid interface, which can then be used to analyze the reaction pathways and mechanisms of adsorption [22, 23]. Three models were used in this research's isotherm study: the Langmuir, Freundlich, and Elovich isotherms:

$$\text{Langmuir equation: } \frac{c_e}{q_e} = \frac{c_e}{q_m} + \frac{1}{bq_m} \quad (2)$$

where $c_e$ is the equilibrium concentration in mg/L, $q_e$ is mass of adsorbate adsorbed by adsorbents at equilibrium in mg/g, $q_m$ is the Langmuir constant for adsorption capacity in mg/g, and the b is the Langmuir constant for adsorption energy in L/mg.

$$\text{Freundlich equation: } \log q_e = \log K_F + \frac{1}{n}\log c_e \quad (3)$$

where $q_e$ is the mass of adsorbate adsorbed by adsorbents in mg/g, $c_e$ is the equilibrium concentration of adsorbate in mg/L, $K_F$ is constant related to adsorption capacity in L/mg, and n is constant related to adsorption intensity.

$$\text{Elovich equation: } \ln\frac{q_e}{c_e} = \ln K_e q_m - \frac{q_e}{q_m} \quad (4)$$

where $q_e$ is the mass of adsorbate adsorbed by adsorbents in mg/g, $c_e$ is the equilibrium concentration of adsorbate in mg/L, $K_e$ is Elovich equilibrium constant in L/mg, and $q_m$ is Elovich maximum adsorption capacity mg/g.

The following three models were used to analyze the kinetics of the adsorption process: pseudo-first-order, pseudo-second-order, and intra-particle diffusion:

$$\text{Pseudo-first-order equation: } \ln(q_e - q_t) = \ln q_e - k_1 t \quad (5)$$

where $q_e$ is the mass of adsorbate adsorbed by adsorbents at equilibrium in mg/g, $q_t$ is the mass of adsorbate adsorbed by adsorbents at the time, t in mg/g, $k_1$ is the rate constant for the Pseudo-first-order model in L/min, and t is time in minutes.

$$\text{Pseudo-second-order equation: } \frac{t}{q} = \frac{1}{k_2 q_e^2} + \frac{t}{q_e} \quad (6)$$

where $k_2$ is the rate constant for the Pseudo-second-order model in g/mg.min, $q_e$ is the mass of adsorbate adsorbed by adsorbents at equilibrium in mg/g, q is the mass of adsorbate adsorbed by adsorbents at the time, t in mg/g, and t is time in minutes.

$$\text{Intra-particle diffusion equation: } q_t = k_p\sqrt{t} + C \quad (7)$$

where $k_p$ is the rate constant for the intra-particle diffusion model in mg/(g.($min^{1/2}$)), C is the constant for the experiment in mg/g, $q_t$ is the mass of adsorbate adsorbed by adsorbents at the time, t in mg/g, and t is time in minutes.

## 3. Results and Discussion

### *3.1. Adsorbent screening and equilibrium study.*

Based on Figure 1, mango leaf adsorbent was found to have the highest adsorption capacity for both copper and silver if compared to decorative palm leaves, longan leaves, and pineapple leaves. The copper adsorption capacity for mango leaves was found to be 22.45 mg/g. As a result, mango leaf adsorbent was selected to be used in the following equilibrium study, batch study, and AAS analysis. The time when there was no noticeable increase in adsorption capacity was called the "equilibrium time," so it was called that, the equilibrium times for copper adsorption were identified as 20 minutes and 30 minutes based on the equilibrium curves.

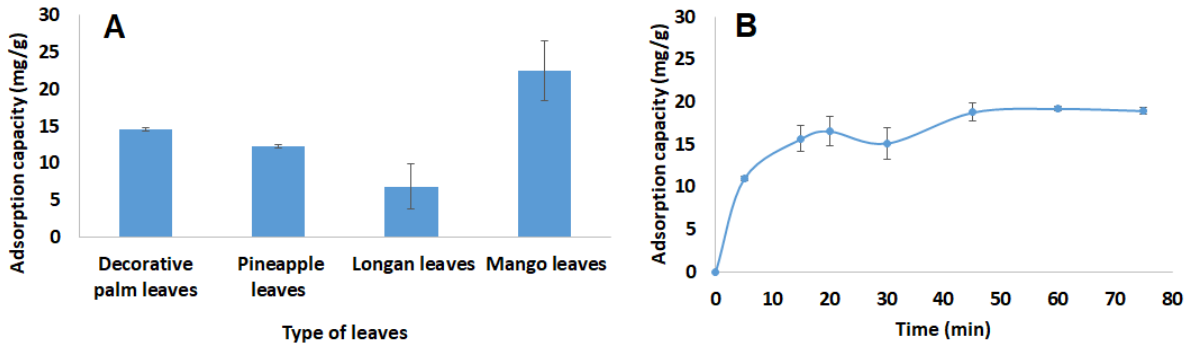


**Figure 1**. (**A**) Adsorption capacity of different adsorbents in adsorbent screening and (**B**) equilibrium curve for copper adsorption.

### *3.2. Batch study.*

According to Figure 2, when the adsorbent dosage was increased, the adsorption capacity decreased because many empty active sites remained available for binding following the adsorption process, resulting in adsorbent waste. Additionally, burying the adsorbents may have occurred due to increasing the adsorbent dosage, resulting in a decrease in adsorption capacity due to some empty active sites for adsorption being buried by the adsorbents on the upper level. The increase in the number of available active sites for heavy metal binding was caused by the decrease in adsorbent aggregation; thus, more heavy metals were allowed to participate in the binding process due to the increased number of available empty active sites, resulting in an increased adsorption capacity. Nonetheless, the increment effect of agitation speed was not evident in Figure 2, which was explained by the study's low adsorbent dosage, ranging from 0.01 to 0.05 g. According to the observed data, the maximum increment in adsorption capacity occurred when the contact time was set to equilibrium. Copper adsorption equilibrium times were determined in this research to be 20 minutes and 30 minutes, respectively. As a result, the maximum adsorption capacity for copper was determined to be 20 minutes. Beyond the equilibrium time, it was discovered that the adsorption capacity remained relatively constant or even increased slightly. In both graphs, the adsorption capacity increased in lockstep with the initial heavy metal concentration. Due to the initial heavy metal concentration increase, more active sites on the adsorbents were allowed to bind with the heavy

metals. Increased utilization of active sites on adsorbents results in an increase in adsorption capacity when the initial heavy metal concentration is higher. The initial heavy metal concentration had an effect on the adsorption capacity by altering the number of adsorbates available for the adsorption process. When the initial concentration of heavy metals was increased, the adsorbents' adsorption capacity was increased [24]. This phenomenon was explained by the fact that more active sites on the adsorbents became entangled with the heavy metals throughout the experiment. As a result, the limiting factor affecting the removal efficiency of heavy metals was the availability of active sites on the adsorbents. When the empty active sites available for heavy metal binding were fully saturated, there was little or no increase in the adsorption capacity of the adsorbents, even when the initial heavy metal concentration was increased further. As a result, the heavy metal removal percentage decreased as the adsorbates' initial concentration increased, despite the increased adsorption capacity [25].

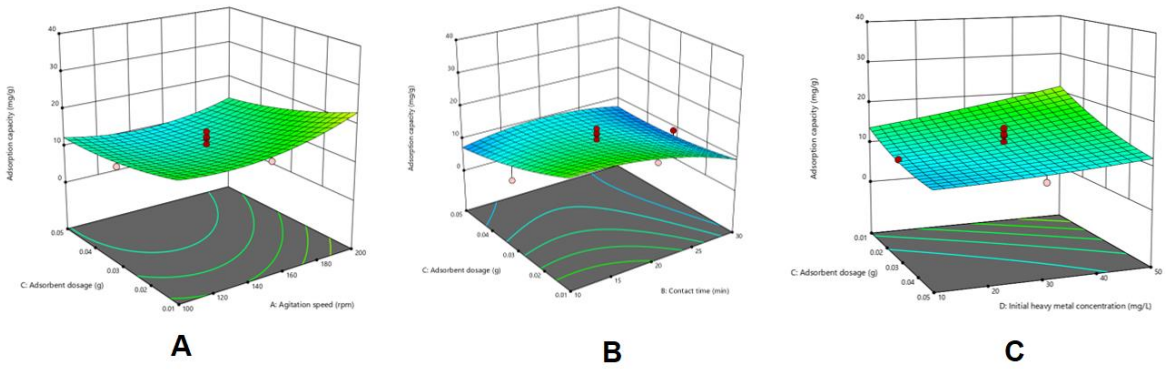


**Figure 2.** 3D surface model graph of (**A**) adsorbent dosage and agitation speed, (**B**) adsorbent dosage and contact time, and (**C**) adsorbent dosage and copper concentration.

Equation 8 illustrates the actual equations generated for copper adsorption. Quadratic models were used to generate the equation. The fitness data was supplied in order to investigate the fit statistics for the generated equation. Copper adsorption has an R2 value of 0.8323. The closer the R2 value is to 1, the more fit the data is to the generated equation:

$$Y_{Cu} = 51.78049 - 0.4404A + 0.025906B - 361.46457C - 0.064531D + 0.003922AB - 1.13244AC + 0.002157AD + 12.15219BC - 0.004415BD - 3.06922CD + 0.001226A^2 - 0.027212B^2 + 3359.42982C^2 + 0.000928D^2 \quad (8)$$

where Y is the predicted adsorption capacity in mg/g, A is agitation speed in rpm, B is contact time in minutes, C is the adsorbent dosage in g, and D is the initial heavy metal concentration in mg/L.

*3.3. FTIR analysis.*

In FTIR analysis, the wavenumbers 400 cm-1 to 4000 cm-1 were classified as the mid-IR spectrum. The fingerprint region was defined between 400 and 1500 cm-1, while the functional group was defined between 1500 and 4000 $cm^{-1}$. The FTIR results for raw adsorbents, adsorbents after copper adsorption, and adsorbents after copper adsorption are plotted in Figure 4 and summarized in Table 2. Within the functional group region, four peaks were observed. For raw adsorbents, the first peak was observed at 3403.6 $cm^{-1}$. The peak was shifted to 3382.56 $cm^{-1}$ following the adsorption process. The peak was identified as an H-bonded OH stretch under hydroxy compound due to its broad nature and wavenumber range of

3570 $cm^{-1}$ to 3200 $cm^{-1}$. The raw adsorbent exhibited a second peak at 2132.04 $cm^{-1}$. After copper adsorption, the peak was shifted to the right by 20.5 $cm^{-1}$. The peak was identified as a terminal alkyne with a monosubstituted carbon-carbon triple bond because the wavenumbers ranged between 2140 and 2100 $cm^{-1}$ [26].

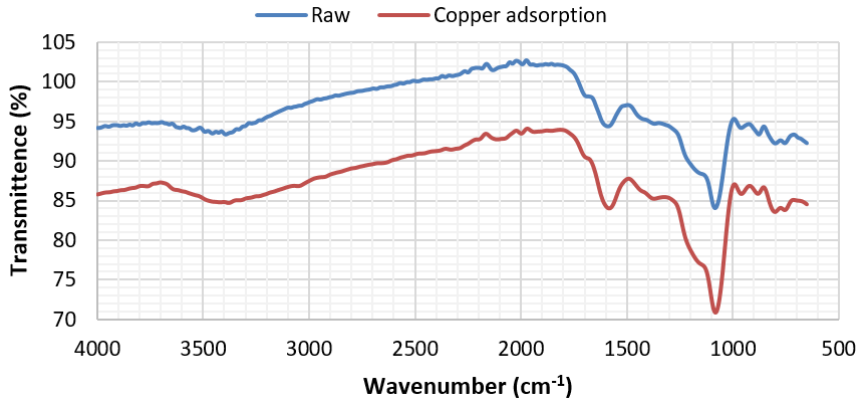


**Figure 3.** FTIR results for raw adsorbents and adsorbents after copper adsorption.

The presence of a second peak established the presence of alkyne as one of the functional groups in the adsorbents. The third peak was determined to be undetectable because the signal from the fourth peak immediately followed it. In raw adsorbents, the third peak was located at 1699.67 $cm^{-1}$. After copper adsorption, the peak was shifted to the left by 1.86 $cm^{-1}$. Due to the wavenumbers being between 2000 and 1660 cm-1, the peak was assigned as aromatic combination bands composed of several substituted aromatic molecules; thus, an aromatic ring in adsorbents was demonstrated by the presence of the third peak. The final peak in the functional group region was observed in raw adsorbents at 1593.44 $cm^{-1}$. The peaks were shifted to 1578.53 $cm^{-1}$ following copper adsorption. The fourth peak was identified as a secondary amine with an N-H bend due to its round tips and location within the functional group of secondary amino between 1650 $cm^{-1}$ and 1550 $cm^{-1}$. The peak was assigned as a C-O stretch under alcohol because the peak located around 1050 $cm^{-1}$ established the presence of primary alcohol [27-29].

**Table 2.** FTIR data for raw adsorbents and adsorbents after adsorption.

| **Wavelength, $cm^{-1}$** | | **Assignment** | **Functional group** |
|---|---|---|---|
| **Raw adsorbents** | **After copper adsorption** | | |
| 3403.6 | 3382.56 | H-bonded OH stretch | Hydroxy compound |
| 2132.04 | 2111.54 | C≡C Terminal alkyne (monosubstituted) | Acetylenic (alkyne) |
| 1699.67 | 1701.53 | Aromatic combination bands | Aromatic ring (aryl) |
| 1593.44 | 1578.53 | N-H bend, secondary amine | Secondary amino |
| 1084.66 | 1080.93 | C-O stretch | Alcohol |

*3.4. Adsorption isotherm and kinetic.*

Figure 4 depicts the adsorption isotherms. The Langmuir isotherm was determined to be the fittest isotherm model for copper adsorptions, with an $R^2$ value of 0.9368. The Langmuir constant was determined to be -0.4869 L/mg for adsorption energy. Thus, the Langmuir isotherm could be used to predict copper's adsorption behavior. The high fitness of the Langmuir isotherm was attributed to the presence of monolayer adsorption in copper via the leaves adsorbent [30-32]. Our results are consistent with previous research, which determined the Langmuir adsorption capacity constant of saffron leaves adsorbent to be 62.96 mg/g, 8.36 mg/g for Hevea brasiliensis leaves adsorbent, and 11.22 mg/g for oil palm leaf powders

adsorbent. Mango leaves adsorbents were found to be more effective at monolayer copper adsorption than Hevea brasiliensis leaves adsorbents and oil palm leaf powders adsorbents but less effective than saffron leaves adsorbents. Nonetheless, different studies used various leaf pretreatments and experimental parameters [33, 34]. The monolayer adsorption capacity comparison results were possibly used to guide future research on the commercial value of various leaf-based adsorbents.

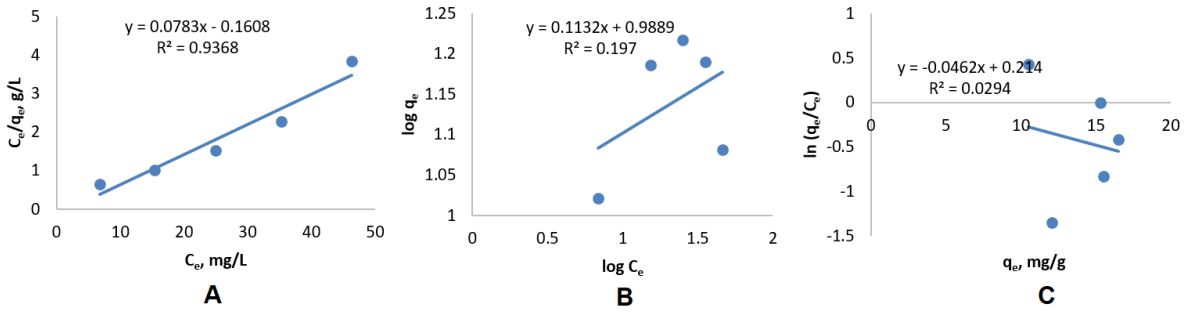


**Figure 4.** Isotherm model for copper adsorption: (**A**) Langmuir isotherm, (**B**) Freundlich isotherm, and (**C**) Elovich isotherm.

Figure 5 depicts the adsorption kinetics models. With an $R^2$ value of 0.534, the pseudo-second-order kinetic model was identified as the fittest kinetic model for copper adsorption. However, the $R^2$ value of 0.534 was considered low compared to 0.9808, indicating that copper adsorption better fit the pseudo-second-order kinetic model. The rate constant for copper adsorption in the pseudo-second-order kinetic model was determined to be 0.005203 L/min. Thus, it was suggested that pseudo-second-order be used to predict the kinetics of copper adsorption.

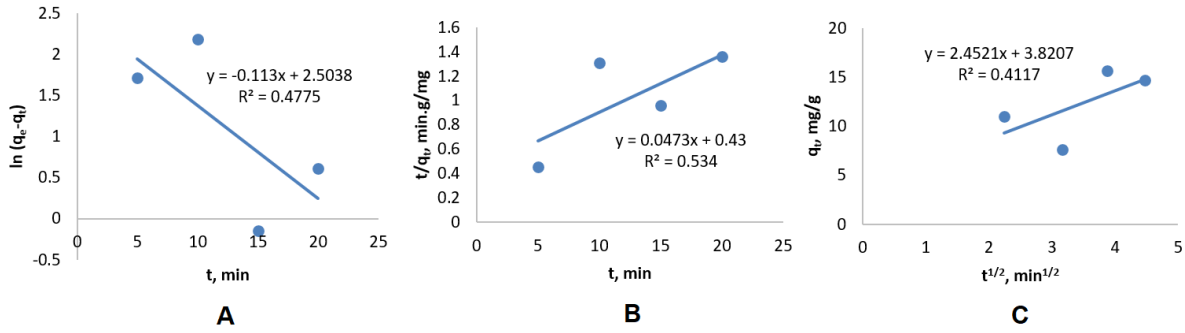


**Figure 5.** Kinetic model for copper adsorption: (**A**) Pseudo-first-order, (**B**) Pseudo-second-order, and (**C**) Intra-particle diffusion.

## 4. Conclusions

The optimum operating condition for copper adsorption was found at 200 rpm of agitation speed, 10 minutes of contact time, 0.01 g of adsorbent dosage, and 50 mg/L of initial copper concentration, where the adsorption capacity was found to be the largest, at 30.6 mg/g. The functional groups of the adsorbents and the effects of adsorption on the adsorbents were successfully identified using the FTIR analysis. The Langmuir isotherm and a pseudo-second-order kinetic model were identified as copper's fittest adsorption isotherm model and adsorption kinetics. This leaf powder is valuable since they are green, economical, and easy to prepare with a simple design biosorption technique.

## Funding

This research was funded by the Faculty of Engineering and Science, Curtin University, through Final Year Project 2019/2020.

## Acknowledgments

The authors thank Curtin University Malaysia for facilitating this study. In addition, the collaboration between Mulawarman University Indonesia and Sejong University Korea is highly appreciated.

## Conflicts of Interest

The authors declare no conflict of interest.

## References

1. Tarfeen, N.; Nisa, K.; Hamid, B.; Bashir, Z.; Yatoo, A.; Dar, M.; Mohiddin, F.; Amin, Z.; Ahmad, R.; Sayyed, R. Microbial Remediation: A Promising Tool for Reclamation of Contaminated Sites with Special Emphasis on Heavy Metal and Pesticide Pollution: A Review. *Processes* **2022**, *10*, 1358, https://doi.org/10.3390/pr10071358.
2. Frichot, J.J.H.; Rubiyatno; Talukdar, G. Water Quality Assessment of Roof-collected Rainwater in Miri, Malaysia. *Trop. Aqua. Soil Pollut.* **2021,** *1*, 87–97, https://doi.org/10.53623/tasp.v1i2.19.
3. Ţurcanu, A.; Matei, E.; Râpă, M.; Predescu, A.; Coman, G.; Predescu, C. Biowaste Valorization Using Hydrothermal Carbonization for Potential Wastewater Treatment Applications. *Water* **2022**, *14*, 2344, https://doi.org/10.3390/w14152344.
4. Yuan, J.; Ding, Z.; Bi, Y.; Li, J.; Wen, S.; Bai, S. Resource Utilization of Acid Mine Drainage (AMD): A Review. *Water* **2022**, *14*, 2385, https://doi.org/10.3390/w14152385.
5. Zhao, C.; Ting, Z.; You, Z.; Kim, H.; Shah, K. Uncontrolled Disposal of Used Masks Resulting in Release of Microplastics and Co-Pollutants into Environment. *Water* **2022**, *14*, 2403, https://doi.org/10.3390/w14152403.
6. Kumar, A.; Tripti; Raj, D.; Maiti, S.; Maleva, M.; Borisova, G. Soil Pollution and Plant Efficiency Indices for Phytoremediation of Heavy Metal(loid)s: Two-Decade Study (2002-2021). *Metals* **2022**, *12*, 1330, https://doi.org/10.3390/met12081330.
7. Qin, G.; Niu, Z.; Yu, J.; Li, Z.; Ma, J.; Xiang, P. Soil heavy metal pollution and food safety in China: Effects, sources and removing technology. *Chemosphere* **2021**, *267*, 129205, https://doi.org/10.1016/j.chemosphere.2020.129205.
8. Alengebawy, A.; Abdelkhalek, S.; Qureshi, S.; Wang, M. Heavy Metals and Pesticides Toxicity in Agricultural Soil and Plants: Ecological Risks and Human Health Implications. *Toxics* **2021**, *9*, 42, https://doi.org/10.3390/toxics9030042.
9. Potter, N.; Meltzer, G.; Avenbuan, O.; Raja, A.; Zelikoff, J. Particulate Matter and Associated Metals: A Link with Neurotoxicity and Mental Health. *Atmosphere* **2021**, *12*, 425, https://doi.org/10.3390/atmos12040425.
10. Munir, N.; Jahangeer, M.; Bouyahya, A.; El Omari, N.; Ghchime, R.; Balahbib, A.; Aboulaghras, S.; Mahmood, Z.; Akram, M.; Ali Shah, S.; Mikolaychik, I.; Derkho, M.; Rebezov, M.; Venkidasamy, B.; Thiruvengadam, M.; Shariati, M. Heavy Metal Contamination of Natural Foods Is a Serious Health Issue: A Review. *Sustainability* **2022**, *14*, 161, https://doi.org/10.3390/su14010161.
11. Galster, S.; Helmreich, B. Copper and Zinc as Roofing Materials - A Review on the Occurrence and Mitigation Measures of Runoff Pollution. *Water* **2022**, *14*, 291, https://doi.org/10.3390/w14030291.
12. Yap, C.; Saleem, M.; Tan, W.; Syazwan, W.; Azrizal-Wahid, N.; Nulit, R.; Ibrahim, M.; Mustafa, M.; Rahman, M.; Edward, F.; Arai, T.; Cheng, W.; Okamura, H.; Ismail, M.; Kumar, K.; Avtar, R.; Al-Mutair, K.; Al-Shami, S.; Subramaniam, G.; Wong, L. Ecological - Health Risk Assessments of Copper in the Sediments: A Review and Synthesis. *Pollutants* **2022**, *2*, 269-288, https://doi.org/10.3390/pollutants2030018.
13. Cepoi, L.; Zinicovscaia, I.; Rudi, L.; Chiriac, T.; Djur, S.; Yushin, N.; Grozdov, D. Assessment of Metal Accumulation by Arthrospira platensis and Its Adaptation to Iterative Action of Nickel Mono- and

Polymetallic Synthetic Effluents. *Microorganisms* **2022**, *10*, 1041, https://doi.org/10.3390/microorganisms10051041.
14. Senze, M.; Kowalska-Góralska, M.; Czyż, K.; Wondołowska-Grabowska, A. Possibility of Metal Accumulation in Reed Canary Grass (*Phalaris arundinacea* L.) in the Aquatic Environment of South-Western Polish Rivers. *Int. J. Environ. Res. Public Health* **2022**, *19*, 7779, https://doi.org/10.3390/ijerph19137779.
15. Adamczyk-Szabela, D.; Wolf, W. The Impact of Soil pH on Heavy Metals Uptake and Photosynthesis Efficiency in *Melissa officinalis*, *Taraxacum officinalis*, *Ocimum basilicum*. *Molecules* **2022**, *27*, 4671, https://doi.org/10.3390/molecules27154671.
16. Bouchelta, C.; Medjram, M.S.; Bertrand, O.; Bellat, J.P. Preparation and characterization of activated carbon from date stones by physical activation with steam. *J. Anal. Appl. Pyrol.* **2008**, *82*, 70-77, https://doi.org/10.1016/j.jaap.2007.12.009.
17. Ho, Z.H.; Adnan, L.A. Phenol Removal from Aqueous Solution by Adsorption Technique Using Coconut Shell Activated Carbon. *Trop. Aqua. Soil Pollut.* **2021**, *1*, 98–107, https://doi.org/10.53623/tasp.v1i2.21.
18. Collivignarelli, M.; Sorlini, S.; Milanese, C.; Illankoon, W.; Caccamo, F.; Calatroni, S. Rice Industry By-Products as Adsorbent Materials for Removing Fluoride and Arsenic from Drinking Water - A Review. *Appl. Sci*. **2022**, *12*, 3166, https://doi.org/10.3390/app12063166.
19. Shaikhiev, I.; Shaykhieva, K.; Sverguzova, S.; Fomina, E.; Vinogradenko, Y.; Fediuk, R.; Amran, M.; Svintsov, A.; Azevedo, A.; Gunasekaran, M. Removing Pollutants from Sewage Waters with Ground Apricot Kernel Shell Material. *Materials* **2022**, *15*, 3428, https://doi.org/10.3390/ma15103428.
20. Salman, M.; Demir, M.; Tang, K.H.D.; Cao, L.T.T.; Bunrith, S.; Chen, T.-W.; Darwish, N.M.; AlMunqedhi, B.M.; Hadibarata, T. Removal of Cresol Red by Adsorption Using Wastepaper. *Ind. Domest. Waste Manag.* **2022**, *2*, 1–8, https://doi.org/10.53623/idwm.v2i1.63.
21. Nandiyanto, A.B.D.; Oktiani, R.; Ragadhita, R. How to read and interpret FTIR spectroscope of organic material. *Indonesian J. Sci. Technol.* **2019**, *4*, 97-118, https://doi.org/10.17509/ijost.v4i1.15806.
22. Azam, M.; Wabaidur, S.; Khan, M.; Al-Resayes, S.; Islam, M. Heavy Metal Ions Removal from Aqueous Solutions by Treated Ajwa Date Pits: Kinetic, Isotherm, and Thermodynamic Approach. *Polymers* **2022**, *14*, 914, https://doi.org/10.3390/polym14050914.
23. Cen, Y.; Li, Y.; Deng, H.; Ding, H.; Tang, S.; Yu, X.; Xu, F.; Zhu, Z.; Zhu, Y. Removal of Copper (II) from Aqueous Solution by a Hierarchical Porous Hydroxylapatite-Biochar Composite Prepared with Sugarcane Top Internode Biotemplate. *Water* **2022**, *14*, 839, https://doi.org/10.3390/w14060839.
24. Mohd Zain, N.B.; Md Salleh, N.J.; Hisamuddin, N.F.; Hashim, S.; Abdullah, N.H. Adsorption of Phosphorus Using Cockle Shell Waste. *Ind. Domest. Waste Manag.* **2022**, *2*, 30–38, https://doi.org/10.53623/idwm.v2i1.81.
25. Wu, X.; Hong, N.; Cen, Q.; Lu, J.; Wan, H.; Liu, W.; Zheng, H.; Ruan, R.; Cobb, K.; Liu, Y. Application of Phosphate Materials as Constructed Wetland Fillers for Efficient Removal of Heavy Metals from Wastewater. *Int. J. Environ. Res. Public Health* **2022**, *19*, 5344, https://doi.org/10.3390/ijerph19095344.
26. Liu, Y.; Chen, Q.; Singh, R. Low-Cost RSAC and Adsorption Characteristics in the Removal of Copper Ions from Wastewater. *Appl. Sci.* **2022**, *12*, 5612, https://doi.org/10.3390/app12115612.
27. Al Anazi, M.; Abdulazeez, I.; Al Hamouz, O. Selective Removal of Iron, Lead, and Copper Metal Ions from Industrial Wastewater by a Novel Cross-Linked Carbazole-Piperazine Copolymer. *Polymers* **2022**, *14*, 2486, https://doi.org/10.3390/polym14122486.
28. Bakalár, T.; Pavolová, H.; Kyšeľa, K.; Hajduová, Z. Characterization of Cu(II) and Zn(II) Sorption onto Zeolite. *Crystals* **2022**, *12*, 908, https://doi.org/10.3390/cryst12070908.
29. Mahyoob, W.; Alakayleh, Z.; Abu Hajar, H.A.; Al-Mawla, L.; Altwaiq, A.M.; Al-Remawi, M.; Al-Akayleh, F. A novel co-processed olive tree leaves biomass for lead adsorption from contaminated water. *J. Contam. Hydrol*. **2022**, *248*, 104025, https://doi.org/10.1016/j.jconhyd.2022.104025.
30. Park, J.H.; Wang, J.J.; Xiao, R.; Wang, M.; Lee, Y.H.; Kang, S.W.; Seo, D.C. Characteristics of adsorption behavior of potentially toxic metals by biochar derived from fallen leaves (Platanus) and its mechanism. *Sustain. Chem. Pharm.* **2022**, *29*, 100776, https://doi.org/10.1016/j.scp.2022.100776.
31. Mathai, R.V.; Mitra, J.C.; Sar, S.K.; Jindal, M.K. Adsorption of Chromium (VI) from aqueous phase using Aegle marmelos leaves: Kinetics, isotherm and thermodynamic studies. *Chem. Data Collect.* **2022**, *39*, 100871, https://doi.org/10.1016/j.cdc.2022.100871.

32. Yin, K.; Wang, J.; Zhai, S.; Xu, X.; Li, T.; Sun, S.; Xu, S.; Zhang, X.; Wang, C.; Hao, Y. Adsorption mechanisms for cadmium from aqueous solutions by oxidant-modified biochar derived from *Platanus orientalis* Linn leaves. *J. Hazard. Mater.* **2022**, *428*, 128261, https://doi.org/10.1016/j.jhazmat.2022.128261.
33. Geng, J.; Lin, L.; Gu, F.; Chang, J. Adsorption of Cr(VI) and dyes by plant leaves: Effect of extraction by ethanol, relationship with element contents and adsorption mechanism. *Ind. Crops and Products* **2022**, *177*, 114522, https://doi.org/10.1016/j.indcrop.2022.114522.
34. Chung, J.H.; Hasyimah, N.; Hussein, N. Application of Carbon Nanotubes (CNTs) for Remediation of Emerging Pollutants - A Review. *Trop. Aqua. Soil Pollut.* **2021**, *2*, 13–26, https://doi.org/10.53623/tasp.v2i1.27.